JOURNAL OF AIRCRAFT
Vol. 45, No. 2, March–April 2008

Flight Testing of the T-Wing Tail-Sitter Unmanned Air Vehicle

R. Hugh Stone,* Peter Anderson,† Colin Hutchison,‡ Allen Tsai,† Peter Gibbens,§ and K. C. Wong§
University of Sydney, Sydney, New South Wales 2006, Australia

DOI: 10.2514/1.32750

Since October 2005, the T-wing tail-sitter unmanned air vehicle has undergone an extensive program of flight tests, resulting in a total of more than 50 flights, many under autonomous control from takeoff to landing. Starting in August 2006, free flights with conversion between vertical and horizontal flight modes have also been undertaken. Although the latter flights have required some guidance-level ground-pilot input, significant portions of them were performed in autonomous mode, including the transitions between horizontal and vertical flight. This paper considers the overall control architecture of the vehicle, including the different control modes that the vehicle was flown under during the recent series of tests. Although the individual controllers for each flight mode are unremarkable in themselves, it is notable that the aggregate system allows the vehicle to fly throughout its entire flight envelope, which is considerably broader than that of conventional fixed- or rotary-wing vehicles. The performance of the controllers for the different flight modes will also be considered, with a particular focus on hover dispersion results, in differing wind conditions. The majority of these flights were performed on a tether test rig during autonomous control development, to ensure vehicle safety with minimal impact on vehicle dynamics. The demonstration of autonomous flight under the constraints imposed by the tether system in winds up to 18 kt is a significant achievement. Results from the more recent horizontal flight tests with conversions between vertical and horizontal flight are also presented. Most important, these results confirm the basic feasibility of tail-sitter vehicles that use control surfaces submerged in propeller wash for vertical flight control.

Nomenclature

$\mathbf{A}$, $\mathbf{B}$	=	state-space system matrices
F_x, F_y, F_z	=	body-axis force components
g	=	acceleration due to gravity
$\mathbf{K}$	=	gain vector
K_Q, K_W, K_{θ_V},K_{IW}	=	control system gains
L, M, N	=	moments about body axes
n_x, n_y, n_z	=	unit vector components
P, Q, R	=	body-axis rates
p_n, p_e, h	=	north, east and height positions
$\mathbf{Q}$, $\mathbf{R}$	=	linear quadratic regular state and control weighting matrices
q_0, q_1, q_2, q_3	=	quaternion components
U, V, W	=	body-axis velocity components
$\mathbf{x}$, $\mathbf{u}$	=	state and control vectors
x, y, z	=	standard body-axis coordinates, centered at the c.g.
δ_e	=	elevator angle (average angle of wing elevons)
δ_{e_W}	=	trim elevator angle per unit of W-translational speed
θ_{V_W}	=	trim vertical tilt angle per unit of W-translational speed
ϕ, θ, ψ	=	standard Euler angles
ϕ_V, θ_V, ψ_V	=	vertical Euler angles
Φ	=	total rotation angle

Subscripts

$()_{\text{comm}}$	=	commanded
$()_0$	=	value taken at reentry to controller

I. Introduction

THE T-wing is a tail-sitter unmanned air vehicle (UAV) that aims to blend the vertical takeoff and landing (VTOL) characteristics and hence operational flexibility of the helicopter with the forward-flight efficiencies of a conventional aircraft in the simplest form possible. Consequently, it uses propeller wash over its wing and fin control surfaces to effect control during vertical flight, rather than cyclic blade pitch variation, as in a helicopter. Furthermore, instead of rotating engines or wings to transition between horizontal and vertical flight, it instead rotates the complete airframe. This makes the vehicle mechanically simpler than other convertiplane designs such as the tilt wing or tilt rotor, while still retaining the ability to fly both vertically and horizontally. A picture of the basic T-wing configuration is shown in Fig. 1, and a typical flight path is given in Fig. 2. The concept-demonstrator version of the T-wing is a 65-lb vehicle, with a wingspan of 7.14 ft, powered by twin 100-cm^3 twin-cylinder two-stroke engines, driving 25-in. counter-rotating fixed-pitch propellers. Other pertinent vehicle parameters are given in Table 1.

The concept-demonstrator version of the T-wing was designed specifically as a research platform to prove the feasibility of controlling such a UAV through its complete flight envelope. Consequently, it only carries 0.528 gal (2 liters) of fuel and its avionics system [inertial measurement unit (IMU), GPS, flight computer, and batteries] accounts for ~20% of its maximum takeoff weight (MTOW). These limitations make the current vehicle unsuitable for real-world applications. Notwithstanding this, other work has been done by Stone [1–3] on developing multidisciplinary configuration optimization software for the preliminary sizing of T-wing-type vehicles up to 1000-lb MTOW, given mission requirements in terms of payload, range, endurance, and hover control performance. Thus, although the current vehicle is only useful as a research platform, [1–3] suggest that the concept has practical merit.

In configuration, the T-wing is most similar to the Boeing Heliwing UAV of the early 1990s [4,5], however, it differs

Received 11 June 2007; revision received 24 September 2007; accepted for publication 24 September 2007.

*Lecturer, School of Aerospace, Mechanical and Mechatronic Engineering, Building J07. Senior Member AIAA.
†Graduate Student, School of Aerospace, Mechanical and Mechatronic Engineering, Building J07.
‡Research Assistant, School of Aerospace, Mechanical and Mechatronic Engineering, Building J07.
§Senior Lecturer, School of Aerospace, Mechanical and Mechatronic Engineering, Building J07.

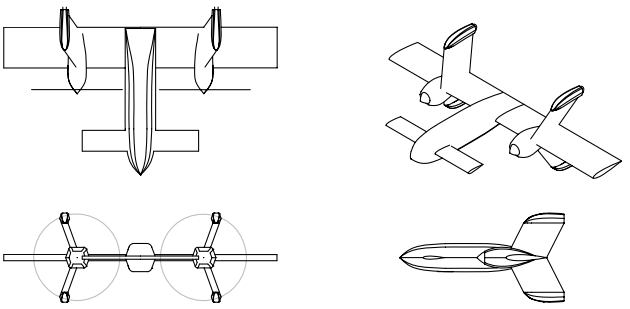

Fig. 1 Generic T-wing configuration: vehicle sits vertically on its fins when taking off and landing; concept-demonstrator fins are not canted.

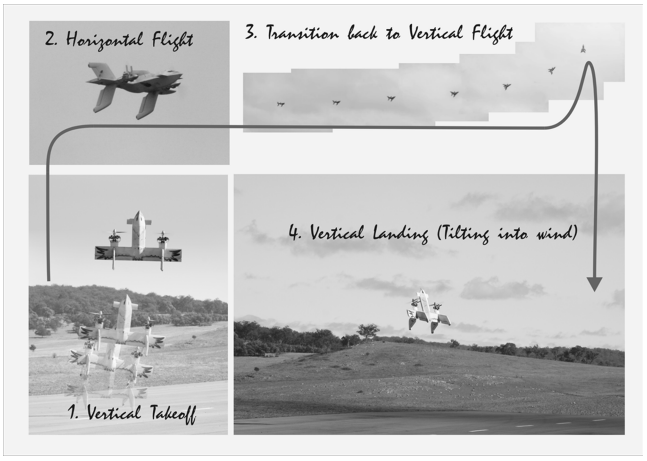

Fig. 2 Composite picture of T-wing UAV; multiple vehicle pictures in some frames are from successive images from a still camera.

fundamentally from that design in its mode of hover control.[¶] Whereas the Heliwing used conventional cyclic rotor controls, the T-wing uses control surfaces submerged in the slipstream of its propellers, similar to the systems used on the manned tail-sitters of the 1950s: the Convair XF-Y1 [6] and Lockheed XF-V1 [7]. These vehicles suffered from hover-mode attitude instability and were difficult to pilot, particularly when landing. By transitioning this original tail-sitter concept to that of an unmanned vehicle and taking advantage of modern electronics to automate the control system, the T-wing aims to obviate these problems and make this original concept a success.

The 1950s and 1960s saw considerable interest in convertiplane vehicles such as tail-sitters. At that time, much of the research was focused on the aerodynamics and basic feasibility of concepts such as the tail-sitter, tilt-rotor, tilt-wing, and ducted-fan types of vehicles. Details of (and references to) much of this work can be found in McCormick [8]. With growing interest in UAVs, many of these VTOL concepts have been revived in unmanned form. Apart from standard helicopter UAVs, the most common VTOL concept appears to be the ducted fan, starting with the Sikorsky Cypher UAV [9] of the early 1990s. Much of the modern research interest in these vehicles has centered on flight control. Avanzini et al. [10] describe a robust control structure for a shrouded-fan vehicle, and Johnson and Turbe [11] describe a dynamic-inversion controller with neural-network adaptation for a smaller ducted-fan vehicle. The latter reference also describes flight tests of the vehicle, including an air deployment by another UAV, an R-MAX helicopter.

Less work appears to have been done on flight control or flight testing of tail-sitter vehicles such as the T-wing. Knoebel et al. [12] describe the modeling of a vehicle substantially similar to the T-wing, though with one central propeller rather than two. Based on some simple aerodynamic modeling, they describe a feedback-linearization control structure that allows their vehicle to fly simulated transition maneuvers as well as hover-flight translations. The most appealing feature of their approach is that attitude control is performed directly in terms of quaternions, which obviates the need for different attitude representations for vertical and horizontal flight, as is done in the present work. Although quaternions and related representations have been used in attitude control for a variety of other aerospace vehicles, including helicopters [13], ducted-fan UAVs [11], spacecraft [14–16], and even the space shuttle [17] back in 1976, their use is particularly appropriate for a tail-sitter UAV that must transition between horizontal and vertical flight. Kubo and Suzuki [18] also present simulation work on developing robust gain-scheduled linear quadratic regulator (LQR) flight controllers for a tail-sitter vehicle. Although the control system design of the T-wing is less sophisticated than the preceding approaches mentioned, flight tests and simulation have shown it to work satisfactorily.

Table 1 Specifications for T-wing concept demonstrator

Property	Value (imperial)	Value (SI)
Wing span	7.142 ft	2.177 m
Wing chord	1.103 ft	0.336 m
Wing leading edge station (from nose)	3.040 ft	0.927 m
Canard span	2.458 ft	0.749 m
Canard chord	0.472 ft	0.144 m
Propeller y position	1.993 ft	0.607 m
Propeller diameter	2.083 ft	0.635 m
Height (standing on ground)	5.000 ft	1.524 m
Engine power (per engine)	7.64 hp	5.70 kW
Takeoff weight (nominal)	65.00 lb	29.48 kg
Total installed thrust (SSL)	~93 lb	~42 kg
Specified maximum hover position excursion (10-kt sharp-edged gust)	2.00 ft	0.61 m

The design of autonomous flight controllers for the T-wing vehicle is complicated by a number of factors. Foremost of these is that the vehicle ranges over a greater variety of flight conditions than a conventional aircraft: from high-speed forward flight through to vertical attitude descent. This means that the aerodynamics associated with this vehicle are both different from and more severely nonlinear than those associated with conventional vehicles. This has necessitated the decomposition of the autonomous flight control problem into four major modes dealing with vertical flight, horizontal flight, and the two transition flight regimes: vertical to horizontal (V2H) and horizontal to vertical (H2V). Further flight control modes are provided to allow different levels of manual control in the event of problems with the autonomous system, as well as to allow for different reversionary modes in case of sensor malfunction. The most challenging flight mode from a control point of view is the vertical flight mode. This is when the vehicle is most unstable and when the aerodynamics and dynamics are least similar to a conventional aircraft. Attempts to fly the vehicle manually in this mode have not been successful. Furthermore, because this is the takeoff and landing mode of the vehicle, it is the most fundamental.

Because of these considerations, most testing of the T-wing to date has been done in vertical flight using a tether test rig to protect the vehicle during control system development. The use of this rig has been vital in allowing the T-wing flight test program to proceed without damaging the airframe. Furthermore, because the vehicle is flown with two tethers and is thus always attached to the ground by (slack) ropes,[**] flight tests can be carried out at smaller, less remote, test sites than are required for free flights. During tethered testing of the vehicle, the focus has been on precise hover control with and without wind, because this is crucial for accurate landing of the vehicle. So far, the vehicle has flown in crosswinds gusting up to 18 kt (30 ft/s).

[¶]The T-wing also differs from the Heliwing in the use of a canard. This surface is currently fixed, though the potential exists to use it for forward-flight control or trim.

[**]The tether ropes weigh 0.108 oz/ft (10 g/m) and are 0.158 in. (4 mm) in diameter.

In addition to the tethered testing of the vehicle, the vehicle has also been flown freely, during which it has performed autonomous takeoffs, V2H and H2V transitions, and horizontal flight. The V2H transitions were accomplished with no significant problems, although some control improvements are still required on the reverse-H2V maneuvers, during which the vehicle experiences angles of attack in excess of 60 deg. Although the vehicle is yet to complete a transition flight with a full autonomous landing, the results to date indicate that this is achievable.

The contribution of the present work is fourfold. First, the flight test results demonstrate the basic feasibility of this type of tail-sitter vehicle in vertical, horizontal, and transition flight modes. Second, these tests and simulation results indicate that a relatively simple control approach can be made to work effectively. Third, the results demonstrate that the aerodynamic modeling of the vehicle [19] is at least sufficiently accurate for control design purposes, without the need for adaptive elements (though these would undoubtedly improve the vehicle's performance). Finally, some readers may be interested in particular details of the tests carried out and the way in which particular problems were solved: for instance, the balancing of engine thrust from side to side, the handling of switching between different control modes, and the like.

This paper is set out as follows. Section II discusses the basic equations of motion of the vehicle, axis systems, and vehicle aerodynamics. Section III outlines the structure of the complete T-wing flight control system, and Sec. IV discusses the physical flight control sensors and hardware. Section V presents simulation results for later comparison with flight test data. Vertical flight test results are presented in Sec. VI, followed by preliminary horizontal and transition test results in Sec. VII. Finally, Sec. VIII concludes the paper with discussion of results to date and an outline of future work.

II. T-Wing Model and Aerodynamics

The T-wing is modeled using the standard 6-DOF nonlinear rigid-body equations of motion as outlined by Stevens and Lewis [19], whose notation will be adopted here. Because of the fact that the propellers are counter-rotating, gyroscopic terms are omitted from the moment equations. Although the use of differential thrust (via differential engine rpm) may introduce minor gyroscopic effects, these will be small and are ignored. The aerodynamic forces and moments required for these equations are supplied through a database that covers more than 4000 flight conditions, ranging over different flow angles α and β, speeds V, and throttle settings δ_T. The database is constructed using an integrated propeller-blade element and panel-method model. This model uses corrections based on measured 2-D viscous data for those regions of the vehicle flowfield well outside the bounds of normal linear aerodynamic analysis [1,20,21]. This allows the vehicle to be modeled for angles of attack and sideslip between ± 90 deg and for velocities ranging from low-speed vertical descent to high-speed forward flight.[††]

The nonlinearities associated with the aerodynamic forces and moments are more extensive than those typically associated with conventional aircraft. This is because the range of flow speeds and angles is greater. A partial appreciation of the force and moment nonlinearities can be gained from a plot of the Z body-axis force, as shown in Fig. 3, taken from the aerodynamic database for the vehicle [21]. In this graph, the four stacked surfaces represent Z force values at different throttle settings plotted against angle of attack and velocity. Stall is clearly seen occurring at $\alpha \approx \pm 20$ deg, after which the four different throttle surfaces separate, due to nonlinear effects.

Unlike conventional aircraft in which the nonlinearity in the force and moment data are largely confined to stall and the parabolic variation of the force terms with speed, the nonlinearities for the T-wing are more complicated, due to the changing relative importance of the propeller-generated forces in comparison with those due to the freestream dynamic pressure. This change occurs as the vehicle goes from low-speed vertical flight (propeller and propeller slipstream forces dominate) to high-speed horizontal flight (freestream lift and drag forces dominate).

[††]The use of negative velocities obviates the need for considering flow angles outside the range of −90 to +90 deg for descending flight conditions.

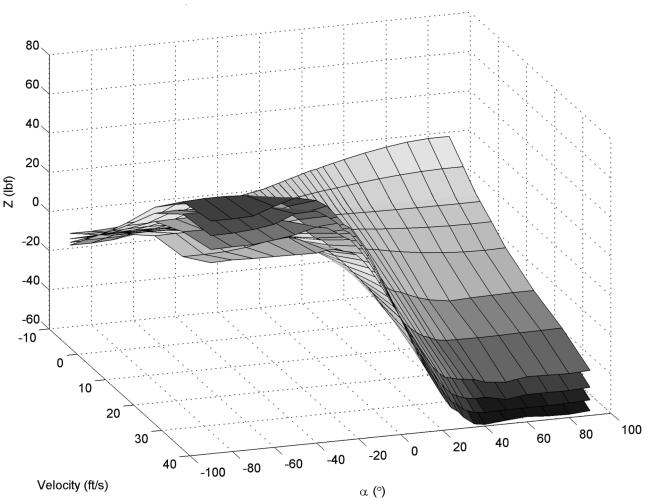

Fig. 3 Z body-axis force plotted versus velocity (fps) and angle of attack (deg) at throttle settings of 0.4, 0.6, 0.8, and 1.0.

A. Attitude Representations

Three distinct attitude representations are used for simulation and flight control of the T-wing vehicle. A quaternion representation is used exclusively in the flight simulation of the vehicle, as well as in the guidance controller for the transition maneuvers between horizontal and vertical flight. The quaternion representation has the advantage of being unique (to within a choice of sign) and of having no areas of degeneracy of its solution. For horizontal flight, the standard Euler-angle rotations of yaw ψ, pitch θ, and roll ϕ are used to describe the vehicle's attitude with respect to the north-east-down (NED) frame. The Euler-angle representation is degenerate at $\theta = 90$ deg, which is problematic for the T-wing because it spends significant amounts of time in a near-vertical attitude.

Because of the degeneracy of the standard Euler angles for vertical flight, it is useful to define a second set of nonstandard Euler angles for vertical mode flight as follows:

1) Start from a vertical attitude with the vehicle belly (z axis) facing north.

2) The vehicle is "rolled" about its longitudinal x axis by a vertical roll angle ϕ_v (opposite sense to ψ).

3) The vehicle is then pitched about its once-moved lateral y axis by a vertical pitch angle θ_v.

4) The vehicle is now yawed about its twice-moved belly z axis by a vertical yaw angle ψ_v to complete the attitude of the vehicle.

Unlike the standard Euler angles, this set is not degenerate when the vehicle is at or near vertical, when the standard pitch angle is close to 90 deg. Furthermore, the sense of all the angles remains consistent between horizontal and vertical representations: roll rate is always about the body x axis, and yaw rate always about the body z axis. If a helicopter attitude convention had been used for vertical mode flight, then the sense of roll and yaw would have varied between the different flight modes. It should be noted that although useful for vertical flight control, this vertical system becomes degenerate when the vertical pitch angle reaches ± 90 deg (horizontal).

Transformations between these three representations can be easily calculated [1]. Similarly, it is also possible to express the kinematic equations of motion in terms of either the vertical or horizontal Euler angles. This is often appropriate when performing control design, because it is more difficult to relate the quaternion representation to physically meaningful control objectives. An alternative method to using two distinct attitude systems for a tail-sitter vehicle has been proposed by Knoebel et al. [12]. They develop guidance and control strategies that cover all flight regimes based solely on a quaternion attitude description, which unifies the control problem. Similar

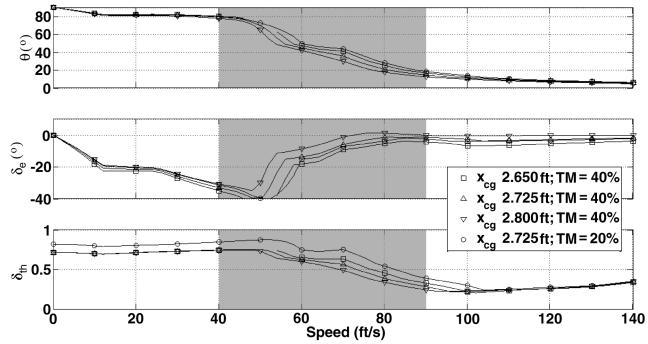

Fig. 4 Predicted trim pitch angle, elevator setting and throttle versus speed for nonclimbing flight; results given for three c.g. locations (measured from the nose) with 40% thrust margin and for mid-c.g. at 20% thrust margin.

approaches for the T-wing have not been used to date (except for transition-mode guidance).

As mentioned in the Introduction, quaternions and other attitude representations have been used for a variety of other aerospace vehicles, including helicopters [13], generic spacecraft [14–16], and the space shuttle [17]. Schuster [22] provides a comprehensive summary of different representations in use across a variety of fields, and Phillips et al. [23] summarize representations in use for aircraft. Although the vertical Euler-angle representation used here for hover-mode flight control lacks the appeal of the unified representation afforded by quaternions, it has been found useful in designing the vertical flight control system for the vehicle and also provides a convenient and meaningful way to describe the attitude of the vehicle in vertical flight.

B. Qualitative Description of Vehicle Characteristics

As indicated in Table 1, the nominal thrust margin for the T-wing vehicle is 40% at standard sea-level (SSL) conditions. Because of variations in density altitude and takeoff weight, some flight tests have taken place with thrust margins less than 20%. Figure 4 shows longitudinal trim characteristics for the vehicle, as predicted using the aerodynamic database [21] for three separate c.g. positions (nominal and one on either side). It also shows the same quantities for a reduced thrust margin of 20%. (Assuming thrust is proportional to density for a normally aspirated piston engine [24], a 20% thrust margin represents the nominal vehicle operating at a density altitude of ~5000 ft.) The kink in the trim elevator angle observed after 12 ft/s is associated with stall onset in one lobe of the propeller slipstream velocity distribution while in (near) vertical flight. Figure 4 shows that it is increasingly difficult for the vehicle to be trimmed vertically in strong winds as the c.g. is moved forward. The results at reduced thrust margin show that despite the higher throttle setting required for vertical flight, the vehicle is clearly flyable in this condition. The shading in Fig. 4 represents the region of greatest uncertainty in the vehicle trim properties. This occurs in the transition region between 40 and 90 ft/s, in which the slipstream regions may be significantly affected by stall and in which the poststall loads from nonslipstream regions become significant. Consequently, there is no intention to try to maintain trimmed flight at these speeds. As mentioned previously, the T-wing is significantly unstable in vertical flight and marginally stable (13% static margin) in forward flight, with a midrange c.g. position.

III. T-Wing Flight Control System

The flight control system for the T-wing consists of a relatively complex amalgam of simple control systems that are used for different autonomous and semi-autonomous flight modes. The fully autonomous modes span the basic operating conditions of the vehicle: vertical, horizontal, and the two transition modes. Further autonomous modes are used to provide some degree of control system fail-safe behavior in the event of particular types of sensor malfunction (such as loss of GPS signal). Another set of semi-autonomous/semimanual modes is provided to allow different levels of ground-pilot intervention during initial flight testing. The major flight control modes and their principal characteristics are outlined in Table 2. The different modes are either selectable from the pilot-control station or are selected automatically in the case of autonomous vehicle transition or failure modes. Because most of these modes use relatively simple gain-scheduled classical controllers designed using frequency-based techniques [19,25,26], no further details will be given as to their structure. In the case of vertical hover flight, however, a brief description of the control structure will be provided. Although these controllers use standard LQR designs [19] made with subspace models of the vehicle dynamics, their description is warranted, due to the relative novelty of the vehicle and the fact that this structure is important when considering reentering this mode after performing a H2V transition.

A. Autonomous Vertical Velocity Mode

During autonomous vertical flight the T-wing uses a set of gain-scheduled LQR translational velocity controllers to control velocities in the body-axis z and y directions using the elevators and rudders, respectively. These are combined with a classical proportional plus integral (PI) vertical roll-angle controller (for heading control or, in other words, in which direction the belly is pointing) and a similar PI vertical velocity throttle controller. The vertical flight mode is when the vehicle is most unstable and also the mode of operation that is most novel in comparison with that of a conventional aircraft.

The following section will briefly consider the design of a vertical attitude translational W-velocity controller for the vehicle. The design of a sideways V-velocity controller is similar. In doing so use

Table 2 Major vehicle control modes

Control mode	Guidance	Low-level control
Autonomous vertical velocity mode	PID waypoint navigation emitting 1) Translational velocity commands 2) Belly pointing angle 3) Climb rate	1) LQR translational velocity controllers 2) PI pointing angle and vertical velocity controllers
Autonomous V2H and H2V transition modes	Quaternion-based attitude guidance emitting P, Q, and R pitch-rate commands	1) Classical P, Q, and R angular-rate controllers 2) Throttle scheduled for transitions
Autonomous horizontal flight mode	Bank-to-turn proportional navigation in two stages: 1) First stage emits climb-rate, bank angle, speed commands; 2) Second stage converts these to P, Q, and R and speed commands	1) Classical P, Q, and R angular-rate controllers 2) Classical speed control via throttle
Autonomous vertical angle mode (for autoland when there is a sustained GPS failure and horizontal velocities are unavailable)	1) Tilt-angle commands either provided by ground pilot or set to zero (for autoland) 2) Vertical speed set by ground pilot or set to −4 ft/s	1) Classical PI tilt-angle controllers 2) PI pointing angle and vertical velocity controllers
Full manual mode (for ground checks only)	Surfaces and throttles directly controlled by the pilot	None

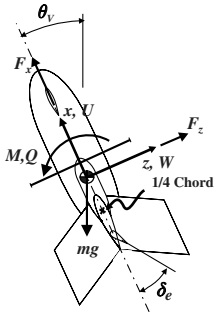

Fig. 5 Vertical flight free-body diagram (all quantities shown positive; belly on the right).

will be made of Fig. 5, which gives a free-body diagram of the vehicle without lateral states.

Using a body-axis system and a vertical pitch angle, as shown in Fig. 5, for the case of nonclimbing vertical mode flight, the equations of motion can be linearized as shown in Eq. (1) [27]:

$$\begin{bmatrix} \dot{W} \\ \dot{Q} \\ \dot{\theta}_V \end{bmatrix} = \begin{bmatrix} \bar{F}_{z_W} & \bar{F}_{z_Q} & -g \\ \bar{M}_W & \bar{M}_Q & 0 \\ 0 & 1 & 0 \end{bmatrix} \begin{bmatrix} W \\ Q \\ \theta_v \end{bmatrix} + \begin{bmatrix} \bar{F}_{z_{\delta e}} \\ \bar{M}_{\delta e} \\ 0 \end{bmatrix} \delta_e \tag{1}$$

In the preceding equation, the force and moment terms are divided by mass and pitch inertia, respectively (represented by overscores), and standard mechanics of flight notation are used to represent the significant force and moment derivatives. No attempt is made to use nondimensional units, due to the problems associated with the choice of an appropriate velocity to use in the nondimensionalizing process. From this equation, the trim elevator deflection and the trim vertical pitch angle per unit of translational velocity W can be easily determined [2,28], as shown in Eq. (2). (Note that in these equations, we use the full force and moment derivatives. This is why "mass" appears in the denominator of the θ_{V_W} equation.)

$$\delta_{e_W} = \frac{-M_w}{M_{\delta_e}} \qquad \theta_{V_W} = \frac{F_{Z_{\delta e}}}{mg}\left(\frac{F_{Z_W}}{F_{Z_{\delta e}}} - \frac{M_w}{M_{\delta_e}}\right) \tag{2}$$

This reduced set of equations can also be used to develop LQR controllers for the vehicle. The equations given in Eq. (1) are in the standard state-space form.

$$\dot{\mathbf{x}} = \mathbf{A}\mathbf{x} + \mathbf{B}\mathbf{u} \tag{3}$$

During flight, the W-velocity component (ft/s), the pitch rate Q (rad/s), and the vertical pitch angle θ_v (rad) are all available for feedback control of the elevator (deg) via the onboard inertial and GPS sensors. Thus, to develop a linear quadratic regulator, all that we require is a state-error weighting matrix $\mathbf{Q}$ and the control effort weighting $\mathbf{R}$. For the current demonstrator vehicle in hover flight in zero wind, the plant matrices are as given next (with imperial units, as indicated before). Typical $\mathbf{Q}$ and $\mathbf{R}$ weighting matrices have also been indicated. This system has an unstable pole located at 1.87 rad/s and a stable pair at $-1.64 \pm 1.99i$ rad/s.

$$\mathbf{A} = \begin{bmatrix} -0.8830.194 - 32.2 \\ -0.385 - 0.5250 \\ 01.0000 \end{bmatrix}; \qquad \mathbf{B} = \begin{bmatrix} -0.241 \\ -0.231 \\ 0 \end{bmatrix}$$
$$\mathbf{Q} = \begin{bmatrix} 1 & 0 & 0 \\ 0 & 0 & 0 \\ 0 & 0 & 0 \end{bmatrix}; \qquad \mathbf{R} = [10] \tag{4}$$

This gives rise to the following control gains on the W-velocity, pitch-rate, and pitch-angle states[‡‡]:

[‡‡]The units of these three gains are deg/(ft/s), deg/(ft/s), and deg/rad for the W, Q, and θ_v states, respectively.

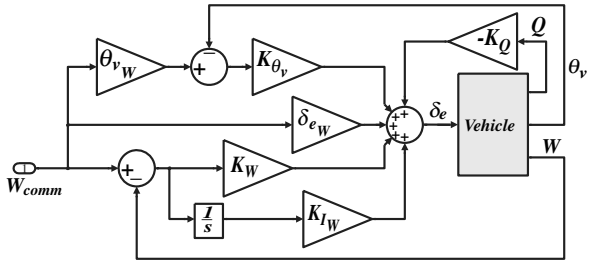

Fig. 6 T-wing W-velocity control system for vertical flight translation.

$$\mathbf{K} = [2.67 \quad -19.0 \quad -46.2] = [K_W \quad K_Q \quad K_{\theta_V}] \tag{5}$$

Using these gains gives a closed-loop system with a gain margin of -8.75 dB, a phase margin of 41 deg, and poles of -1.88 and -1.64, $\pm 2.00i$. The regulator is converted into a controller by simply regulating the error between a commanded and actual velocity. Such a controller will typically not have zero steady-state error. To fix this, the trim values for the tilt angle θ_v and the elevator deflection δ_e are used in a modified control law, which ensures that the steady-state value of the elevator deflection is exactly what is required for flight at the given velocity. The addition of an integral W state to the controller then provides robustness against modeling errors and disturbances:

$$\begin{aligned} \varepsilon_W &= W_{\text{comm}} - W \\ \delta_e &= K_W \varepsilon_W + K_{IW} \int \varepsilon_W \, \mathrm{d}t - K_Q Q \\ &\quad + K_{\theta_V}(\theta_{V_W} W_{\text{comm}} - \theta_V) + \delta_{e_W} W_{\text{comm}} \end{aligned} \tag{6}$$

In actual flight tests, controllers with and without the integral term were used. A block diagram of this controller is given in Fig. 6. The integral term in Eq. (6) may cause problems because constant (or average) wind disturbances occur in the fixed NED frame, whereas the integral error (as written) is stored in the body-axis frame. Thus, during a pirouette, an average wind-disturbance error related to a particular orientation is carried into another orientation. This may cause a significant transient while the integral state adapts to the disturbances in the new orientation.

The gains used in this controller are scheduled with vertical flight speed and throttle setting. A better scheduling parameter would be the prop-wash dynamic pressure. Unfortunately, this is hard to measure explicitly and must be inferred from vertical speed, throttle setting, and (if available) local relative wind. The design of the sideways translational V-velocity controller is exactly analogous, except that we include differential thrust using a proportional gain tied to rudder deflection. This gain is currently set at 0.006/ deg. Thus, at full rudder deflection (38 deg) this gain leads to a $\sim$24% throttle-setting imbalance from side to side. This particular feature of the control system is hard to design accurately, because it requires knowledge of the engine time constants. For this reason, the proportional interconnect between the rudder and differential throttles was chosen based on achieving acceptable simulation results over a range of conditions, with values confirmed via flight test.

Fully autonomous vertical flight involves the UAV navigating between a set of points in space that are defined before takeoff. The waypoint definition involves specifying the Cartesian coordinates of each point as well as the belly-pointing angle of the UAV. By altering the pointing angles at different waypoints, the UAV can be instructed to translate between points in a flatwise (W velocity) sense, sideways (V velocity), or in any skewed combination of these. Furthermore, by specifying waypoints with different pointing angles but the same spatial coordinates, the vehicle can be made to perform pirouettes. Guidance in autonomous vertical flight is provided by proportional plus integral plus derivative (PID) guidance controllers in the local-vertical, local-horizontal frame, to keep the UAV on a track between the previous waypoint and the next one. The outputs of these

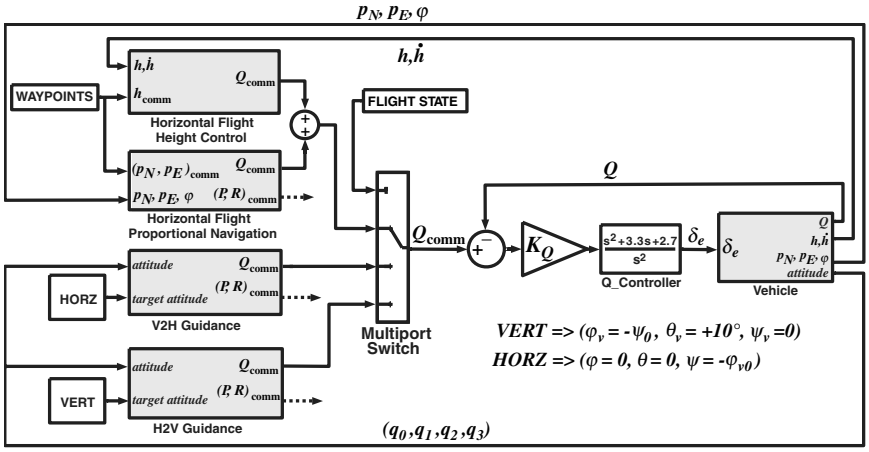

Fig. 7 Pitch-rate control for horizontal flight and transition maneuvers.

guidance controllers are limited to help avoid control surface saturations in the low-level controllers.

B. Autonomous Transition Flight Modes

The V2H and H2V transition flight modes use low-level classical angular-rate controllers combined with attitude guidance based on quaternions. The controller for pitch rate is shown in Fig. 7. The K_Q gain in this controller is scheduled with speed and throttle setting, and antiwindup limits are placed on the internal controller integrator states. This figure also shows the guidance blocks that generate the pitch-rate commands for horizontal flight and the transition maneuvers. On entering a transition maneuver, the error between the current attitude and the desired attitude is expressed as a quaternion. The normalized vector part of the error quaternion, $[n_x, n_y, n_z]^T$, gives the unit rotation vector required to achieve the attitude change. Using this vector (expressed in body axes) multiplied by the product of the total rotation angle Φ (also obtained from the quaternion) and a guidance gain then gives the appropriate angular-rate commands required for the attitude change. This is shown in Eq. (7) and is exactly the procedure outlined by Knoebel [12].

$$\mathbf{q}_{\text{err}} = \begin{bmatrix} q_0 \\ q_1 \\ q_2 \\ q_3 \end{bmatrix} = \begin{bmatrix} \cos(\Phi/2) \\ n_x \sin(\Phi/2) \\ n_y \sin(\Phi/2) \\ n_z \sin(\Phi/2) \end{bmatrix} \qquad \begin{bmatrix} P_{\text{comm}} \\ Q_{\text{comm}} \\ R_{\text{comm}} \end{bmatrix} = K_\Phi \Phi \begin{bmatrix} n_x \\ n_y \\ n_z \end{bmatrix} \tag{7}$$

An alternative simpler method for transition maneuver guidance is to command a pure pullup (H2V) or pure pushover (V2H) at a fixed (or scheduled) pitch rate until a target attitude is attained. Although this only works if the vehicle enters the maneuvers with its body x–z plane approximately vertical, this is not a major restriction. This was the procedure adopted in the horizontal flight test detailed later. For the V2H transition, the throttle is set to 100%, whereas for the reverse H2V transition, the throttle is scheduled with forward speed to balance conflicting requirements of maintaining adequate airflow over all control surfaces versus limiting the total height gained in the maneuver.

C. Autonomous Horizontal Flight Mode

The autonomous horizontal flight mode uses the same angular-rate controllers as for the transition maneuvers at the lowest level and a proportional navigation bank-to-turn guidance algorithm [25]. The guidance algorithm emits bank-angle, climb-rate, and velocity commands. The bank-angle and climb-rate commands are further converted to angular-rate commands, which are then sent to the low-level classical P, Q, and R controllers. This structure is used because it means that the low-level controllers are common between the horizontal and the V2H and H2V transition modes. For this reason, there are no significant control transients when switching between the horizontal and transition flight modes and no need to reset the integrator states within the angular-rate controllers. The switch from V2H to horizontal guidance occurs automatically when the pitch angle passes through 15 deg. The switch from horizontal to H2V guidance occurs automatically when the vehicle passes through a horizontal waypoint and detects that the next waypoint is vertical (indicated by a flag value attached to the waypoint).

D. Autonomous Mode Switching

At the start of the V2H transition and the end of the H2V transition it is necessary for the vehicle to change its low-level controllers. Of these two cases, simulation and experience have shown that the most serious mode switch arises at the top of the H2V transition, in which the vehicle reenters direct translational velocity control. This mode change is triggered 2 s after the vehicle passes through the vertical on its way to its target oververtical attitude $\theta_v = 10$ deg. This mode change gives the greatest problems, because at the top of the transition, the vehicle typically still has significant translational velocity, and the control settings and states will be a long way from trim values desired by the guidance system. To overcome extreme control transients at this point, the following procedure is used:

1) At entry to vertical velocity mode, the current value of the control surface setting and the relevant states of the vehicle are recovered. If present, the integral velocity error state is set to zero.

2) Eq. (6) is then used to backcalculate the W command that corresponds to the current states and control surface setting at entry to the vertical flight mode, given the known gains of the controller, as shown in Eq. (8):

$$W_{\text{comm}_0} = \frac{K_W W_0 + K_Q Q_0 + K_{\theta_V} \theta_{V_0} + \delta_{e_0}}{K_W + \delta_{e_W} + K_{\theta_v} \theta_{v_W}} \tag{8}$$

3) This W command is then ramped down to zero over 5 s to bring the vehicle to a stable hover.

4) A similar procedure is used for the lateral translational V-velocity command.

5) After this, vertical waypoint guidance proceeds as normal.

This procedure appears to work well in simulation and also in flight test. An alternative procedure to achieve bumpless transitions between flight modes is to initialize a controller integrator state to a value that corresponds to both the current control surface setting and the current states and commands. An example of the use of this technique for controllers in a highly maneuverable helicopter is given by Gavrilets et al. [29]. Such a technique was not applicable here, because the vehicle was not always flown with integral states in the W and V controllers.

IV. Flight Control System and Hardware

The vehicle has a simple but accurate suite of onboard sensors to enable it to estimate its current state. A schematic of this system is

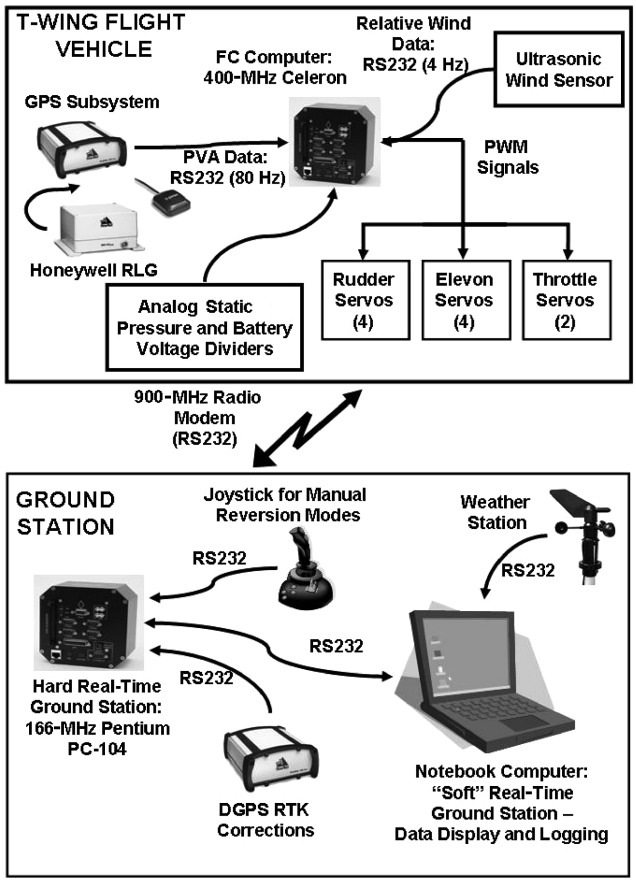

Fig. 8 T-wing flight control system.

shown in Fig. 8. The flight control system consists of a 400-MHz Celeron flight computer in a PC-104 form factor; a Honeywell HG1700AG17 Ring-Laser Gyro IMU; a Novatel ProPak-G2 Plus 5-Hz GPS receiver, which includes a dedicated Kalman filter to interface with the Honeywell IMU to give filtered position, velocity, and attitude (PVA) estimates; and an analog-to-digital converter to monitor battery voltages and the static pressure sensor. A 900-MHz radio modem is used to communicate with the ground station. All significant state data are transmitted and recorded at 80 Hz. As an option, the vehicle can be flown with a Gill Instruments Windsonic ultrasonic wind sensor mounted on the nose of the vehicle. This measures V and W components of relative wind at the nose at a rate of 4 Hz and a resolution of 0.1 m/s.

The current flight control system with RTK GPS provides position estimates with 2-cm errors and velocities within 2 cm/s. Although the system occasionally reverts to plain differential mode (with position accuracies of 1 m), the relatively high-quality IMU means that short-length dropouts can be tolerated before errors grow too large and that long-term dropouts only lead to slow drifts between true and measured positions. The IMU also provides precise angular measurements, with quoted accuracies of 0.05 deg. Although this level of accuracy is not required for a general tail-sitter vehicle operating freely, it is required for fully autonomous flight within the limited confines of the tether test rig, because significant state errors can lead to position biases, which may place the vehicle beyond the bounds of the test rig. To date, the vehicle has not been equipped with an air data system other than a simple static pressure sensor. Some hover-mode flights were conducted with an ultrasonic wind sensor mounted on the nose (see Fig. 9); however, the shape of this sensor precludes its use for forward flight.

V. Simulation Results

Although this paper is focused on the flight testing of the T-wing, a few simulation results will be presented for comparison with the flight test data. Results will be given for one hover and one forward-flight condition. To allow useful comparisons, wind measurements from the flight tests given later were imported into the simulations. These measurements were obtained at the ground station, ~60 ft from the takeoff and landing point. Their use ensures that the simulated conditions are comparable with (if not exactly the same as) those encountered by the vehicle during test.

Fig. 9 Vehicle in hover-mode flight in wind with ultrasonic wind sensor on nose.

A. Vertical Flight Simulation

For all hover tests a standard + flight pattern was used, each leg being 8 ft, for a total width of 16 ft. This pattern involves a total of 27 waypoints that the vehicle must pass through and exercises as much of the vertical flight functionality as possible within the confines of the tether test rig (described later). This functionality includes translations, skewed translations, pirouettes, climbs, and descents. The capture tolerance for waypoints is 6 ft in position and 10 deg in pointing angle. Although the position tolerance seems large in comparison with the + dimensions, the vehicle dwells at each waypoint for 6 s after capture, during which time it still tracks toward that waypoint. To force the vehicle to land, the last waypoint is simply placed 1 ft below ground. The standard test pattern is as follows:

1) Climb to 10 ft (3.05 m), with the vehicle belly (z body axis) pointing north.

2) Maintain this altitude and orientation and fly a + pattern with 8-ft (2.44-m) legs in each direction.

3) Return to center and reorient the vehicle with the belly pointing north–east.

4) Maintain this orientation and fly the same + pattern as in step 2 (but now all translations involve a combination of W and V commands).

5) Reorient the vehicle with the belly pointing north and perform a clockwise pirouette (N → E → S → W → N) about the center point, with stops at each compass leg, followed by a similar anticlockwise pirouette.

6) Climb to 12 ft (3.66 m); descend to 4 ft (1.22 m); then land.

Results from performing a simulation using the wind data from the flight of 18 July 2006 are given in Figs. 10 and 11. The wind inputs are shown in Fig. 12 and reach speeds of ~18 kt (~30 ft/s). The simulation position results (Fig. 10) show that in these winds the hover precision has a 2σ bound of 5.32 ft. Significant position deviations are observed during the pirouettes. The vertical pitch- and

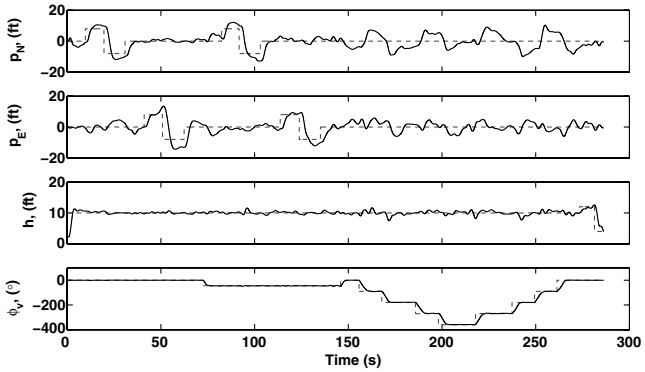

Fig. 10 Simulation position states and belly-pointing angle ϕ_v using the same wind as for the 18 July 2006 flight; $\sigma = 2.66$ ft.

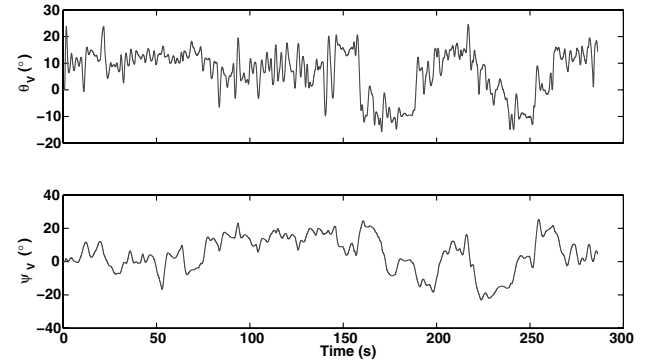

Fig. 11 Simulation vertical Euler pitch and yaw angles using the same wind as for the 18 July 2006 flight.

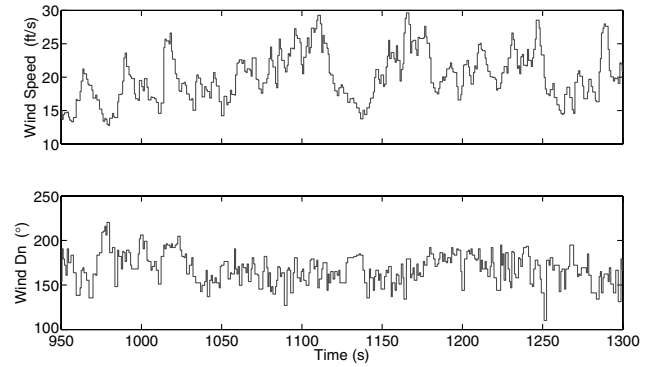

Fig. 12 Wind speed and direction for 18 July 2006; wind between 15 and 30 ft/s (9–18 kts), mainly from the south; time base reflects the test data file: for simulation, the time base was shifted by 950 s.

yaw-angle results given in Fig. 11 show the vertical pitch angle varying in the range of −15 to 25 deg.

B. Horizontal Flight Simulation

Simulation results for a complete flight involving both transitions between horizontal and vertical flight are presented in Figs. 13–15. Wind data were taken from the actual transition flight of 30 August 2006 and varied between 13 and 20 ft/s (7.8 to 11.6 kt). Figure 13 shows a plan view of the simulated flight path and Figs. 14 and 15 show details of the pitch attitude, velocity, and height. The vehicle is seen to climb slightly during the V2H transition (Fig. 14) and gains approximately 120 ft during the reverse-H2V transition (Fig. 15). The extra 80-ft climb at the end of the H2V transition is to enable the vehicle to pass through a waypoint at 400 ft and is not part of the transition maneuver per se. Other work by Stone [30] on transition maneuver optimization has shown that unstalled H2V

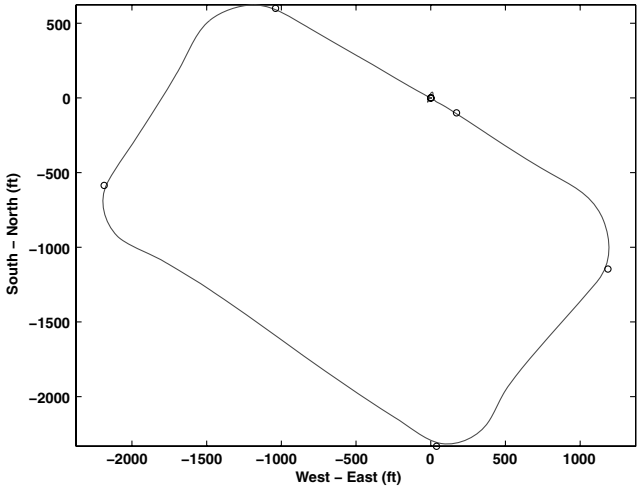

Fig. 13 Simulated horizontal flight pattern with wind as measured during the flight of 30 August 2006 (waypoints are indicated with circles).

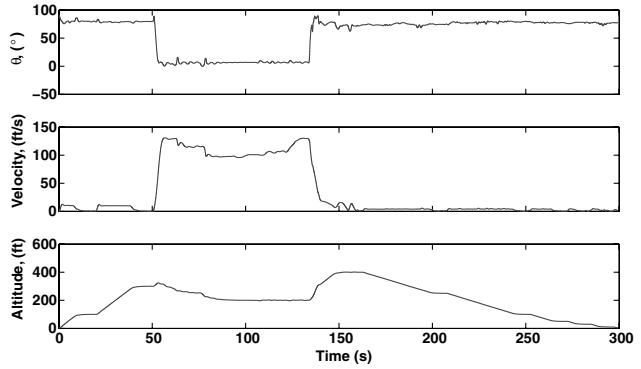

Fig. 14 Pitch-angle, velocity, and altitude profiles for simulated horizontal flight pattern.

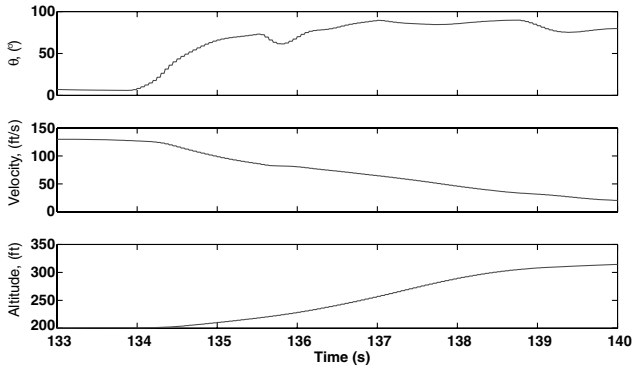

Fig. 15 Pitch-angle, velocity, and altitude during transition for simulated horizontal flight pattern.

transitions can be completed in ∼300-ft altitude gain without breaking a 12-deg angle-of-attack boundary until a specified exit translational speed is reached. This more conservative transition was not used in the present tests, because it would add ∼75 s to the descent time.

VI. Vertical Flight Tests

The analysis of results from the recent T-wing vertical flight test campaign (from October 2005 to August 2006) will focus on the hover precision of the vehicle in both windy and calm conditions. Before describing test results, some aspects of the test procedure will be detailed.

A. Tether Test Rig

The tether test rig used for the vertical flight tests consists of a 66-ft (20-m) aluminium pole erected at a 45-deg angle to give a working height for flight tests of approximately 46 ft (14 m). Figure 16 shows the basic rig, and Fig. 17 presents a picture from an actual flight test.

The usable envelope for tether tests is significantly less than 46 ft to ensure that no part of the vehicle can contact the tether pole and to allow attachment of a weight on the tether rope above the vehicle. This ensures that when descending, the vehicle does not directly pull rope through the top pulley. A bottom tether rope is also used (attached to the ground) to limit the maximum height that the vehicle can fly. This is given a length of ~16 ft (5 m). Flying at 10 ft (3 m) above the ground gives the vehicle a 13-ft (4-m) sideways envelope to move in.

B. Tilt Calibration of Engines

The T-wing currently uses two Desert Aircraft DA-100 engines driving 25 × 10 in. Garvin wooden fixed-pitch propellers. During initial autonomous flight control tests, one problem that soon became apparent was engine thrust variability. Variations were observed both in total installed thrust and between the port and starboard engines on a day-to-day basis. Some of the reasons for these variations are as follows:

1) There were different atmospheric conditions between test days.

2) There were slight differences in the tuning of the two-stroke engines.

3) There were variations in the propellers. [Although the contra-rotating propellers are manufactured by a numerically controlled (NC) milling machine, significant performance variations are still observed between them. This is most likely due to slight differences in the torsional stiffness characteristics of the wood, resulting in differing amounts of twist under load.]

4) Wind variations can lead to takeoff throttle differences in excess of 10% from day to day.

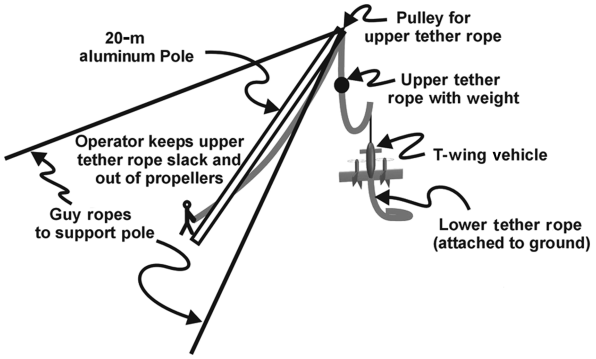

Fig. 16 Tether test-rig setup.

Fig. 17 Tether test rig with T-wing flying below; both tethers are slack; first author is to the left, managing the tether rope.

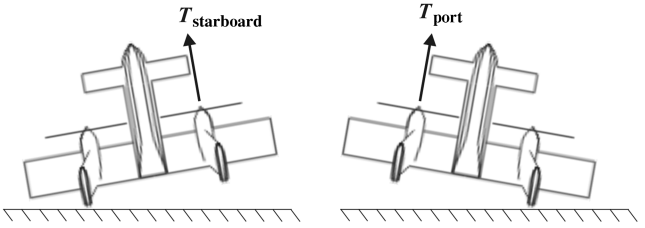

Fig. 18 Tilt calibration of engines (fins are not canted on the concept demonstrator).

To overcome these problems, the T-wing currently performs an autonomous throttle tilt calibration before all flights. This procedure is invoked after engine start. First, the port engine autonomously ramps up at a rate of 3%/s while the starboard engine is held at idle (20%). When the IMU detects a tilt angle of 3 deg, the throttle setting is recorded and then the engine is reduced to idle. A similar procedure is then performed on the starboard engine. Because the landing gear are directly below the engines, the throttle settings so recorded are the hover thrust settings required for flight on that day. Although this procedure ignores ground-effect contributions, these are known to be small. A picture of the procedure is given in Fig. 18.

A further use for the tilt-calibration procedure is the determination of the total excess thrust available to the vehicle. This can be done by simply repeating the tilt-thrust calibration while steadily adding weights to each nacelle. When a given engine is no longer able to lift its side with the throttle at 100%, the maximum thrust point for that side has been exceeded.

The tilt-calibration procedure was of significant use in determining feedforward-trim hover throttle settings for balanced flight. Errors in the calibration are covered by the rudder-to-differential throttle interconnect described earlier (which also provides extra yaw-control authority). One deficiency of the tilt-calibration procedure occurs when operating on a windy day with the wind blowing along the axis of the wings (y body axis). In this case, the windward engine may "see" a higher wind than the downwind engine, which may be partially blanked by the fuselage. Because any crosswind helps increase the engine thrust at a given throttle setting, the tilt-calibration may be biased toward the windward engine. Once the vehicle takes off and alters its orientation, this bias in feedforward-trim differential throttle must be overcome by the control system.

C. Hover Tests: Dispersion in Moderate Winds

Figures 19–21 show the hover performance of the vehicle in performing the standard + pattern maneuver. The plan-view plot (Fig. 19) shows the vehicle track over a full autonomous flight conducted on 13 July 2006, including pirouettes, and shows no sign of biases with a 2σ hover precision of less than 2.5 ft. This flight was conducted in winds of 6–8 kt. Figure 20 shows the actual position-state traces for this flight. The position doublets are clear and show no significant difference between skewed and nonskewed translations. The winds during this test as measured *at the ground station* are given in Fig. 21. The only slight problem with this particular test is that the vehicle became stuck on one of the reverse pirouette waypoints for approximately 170 s. This was due to the integral state in the pointing-angle controller being inactive for this particular flight. Simulation results (not shown here) using the wind data from this flight show comparable position errors, with a slightly higher 2σ bound of 2.88 ft and more wander during the pirouettes.

D. Hover Tests: Dispersion in Strong Winds

The vehicle was also flown using the standard + pattern in winds up to 18 kt (see Fig. 12). Plots for this are shown in Figs. 22–24.

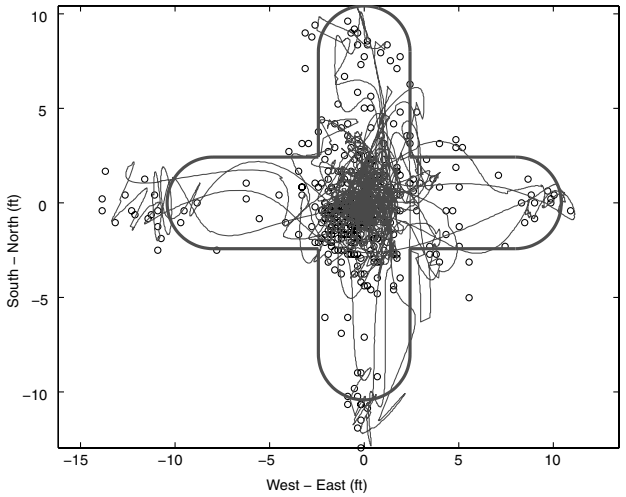

Fig. 19 Plan-view position plot for normal hover flight on 13 July 2006; winds at ∼6–8 kt; plot covers full flight including both + patterns and both pirouettes (bounding cross indicates 2 − σ error variation for flight path); σ = 1.21 ft.

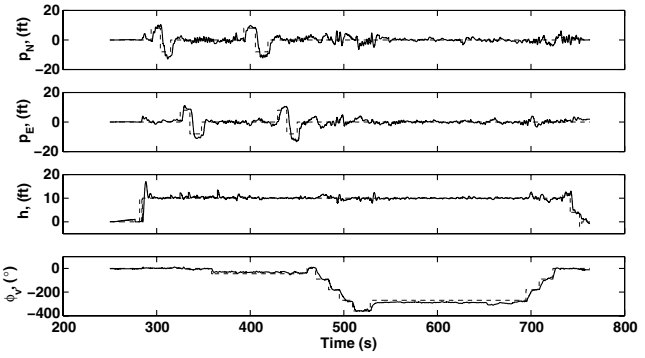

Fig. 20 Position states during hover tests (commanded positions dashed); north and east doublets are clear. In the first doublet, the vehicle belly is facing north and the vehicle moves N → S → N → E → W → E; in the second doublet, the vehicle is skewed facing NE, but the vehicle performs the same N → S → N → E → W → E doublet cleanly.

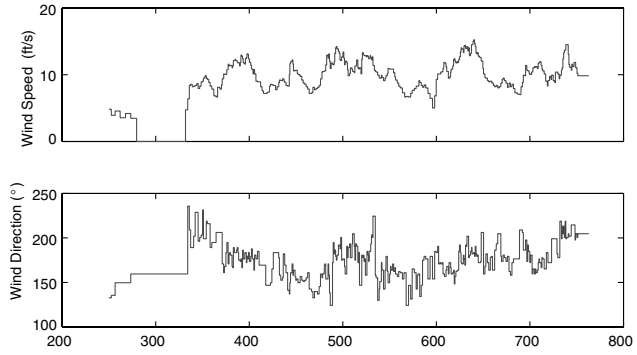

Fig. 21 Wind speed and direction between 8 and 14 ft/s (6–8 kt) from the south (measured at the ground station ∼60 ft from the takeoff point).

Although the precision is clearly less than before (this time the 2σ error bound is 5.58 ft), it is reasonable considering the strength of the wind. The error is also commensurate with the original design specification for the vehicle, which required a maximum 2.0-ft position deviation during hover in the presence of a 10-kt (17 ft/s) sharp-edged gust. Figure 23 also shows the obvious pirouettes ϕ_V that occur between 1130 and 1240 s. Finally, Fig. 24 shows the vertical Euler tilt angles during this flight. From this plot, the large

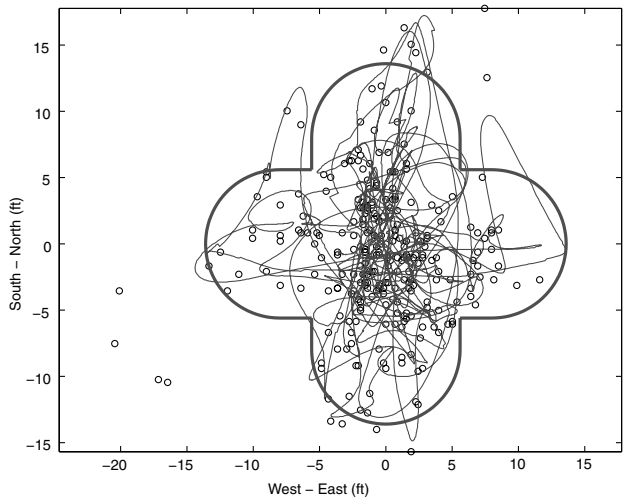

Fig. 22 Plus pattern plan view (ft) in strong winds; plot covers full flight, including both + patterns and both pirouettes; σ = 2.79 ft (thick lines indicate 2σ error bounds).

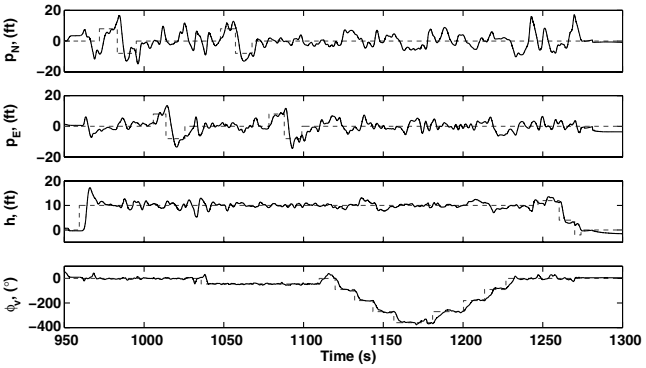

Fig. 23 Position states (ft) for plus pattern in strong winds (commanded position doublets dashed); hover precision is clearly less than for the moderate-wind case.

pitch θ_V tilt angles (up to about 40 deg) that are required to hold position in this wind are clear.

Comparing these results with the simulation (Figs. 10 and 11), the hover precision is marginally worse, and the responses (particularly, the vertical pitch angle) exhibit less damping and greater excursions than in the simulation. These discrepancies point to possible errors in the aerodynamic database, though the presence of experimental imprecision (such as significant engine vibrations causing filter errors) may also be important. The vertical pitch angle also shows a

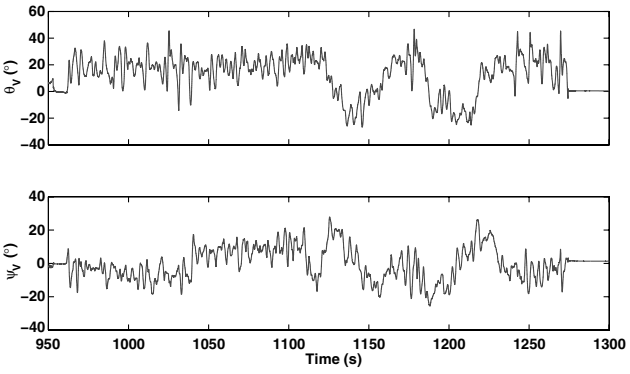

Fig. 24 Vertical Euler angles in strong winds; the θ_v tilt angle (angle away from vertical) reaches 40 deg at some points when the belly is opposite the wind (belly facing north and wind from the south).

different trim bias in the test, which is probably due to a z-wise c.g. offset toward the belly of the vehicle, causing an increase in the trim vertical pitch angle.

VII. Horizontal and Transition Flight Test Results

During August 2006, the first three transition and horizontal flight tests of the T-wing were conducted. A further horizontal flight was also conducted in February 2007. To date, the T-wing has completed autonomous takeoffs, V2H transitions, horizontal transitions, and H2V transitions. Some problems were encountered at the top of the H2V transition, due to issues with rudder gain scheduling and the extreme angles of attack encountered. Landings have thus been performed with pilot-assisted guidance-level control. The data presented here show various qualitative aspects of the T-wing horizontal and transition flight performance.

Figure 25 shows the flight path of the vehicle for the flight on 30 August 2006,[§§] overlaid on an aerial photograph of the University of Sydney Marulan test site. Graphs of pitch-angle, velocity, and altitude for the complete flight are provided in Fig. 26. This flight consisted of the following phases: 1) autonomous takeoff and tracking through two vertical waypoints: one at 100 ft and the other at 300 ft, 2) autonomous transition to horizontal flight, 3) autonomous tracking through the first horizontal flight waypoint and turn to track the next waypoint, 4) pilot guidance-level intervention at the end of this turn to correct altitude loss (due to a complicated interaction between underpredicted drag and gain scheduling of the pitch-rate controllers), 5) performance of first H2V transition semi-autonomously followed by a commanded V2H transition and a further pilot-guided circuit, and 6) performance of second H2V transition semi-autonomously followed by descent to landing under pilot guidance-level control.

In the preceding description, the H2V transitions are described as *semi-autonomous* because the pilot stick input (which maps to vehicle pitch-angle commands during pilot-assisted horizontal flight) is set so that full backstick is treated as a logic signal, forcing the vehicle to perform a transition maneuver. Provided backstick is maintained through the maneuver, the maneuver guidance is autonomous until a vertical attitude is reached.

This flight demonstrates a variety of important characteristics of the concept-demonstrator version of the T-wing.

A. Altitude Loss in the V2H transition

The total altitude loss in the first V2H transition was ∼10 ft. Furthermore, because the vertical flight guidance of the vehicle requires that it dwells for 3 s[¶¶] at each vertical mode waypoint, the vehicle performed this transition virtually from a standing start. (The total velocity at entry was 3.61 ft/s). This result shows a slight difference with the simulation data, in which the vehicle climbed slightly through the transition. This suggests that the simulation overpredicts the total engine thrust, particularly at the top end of the throttle.

B. H2V Transition Details and Mechanism

In the final H2V transition, the total height gain was ∼80 ft. A detailed graph of the pitch-angle, velocity, and altitude states is provided for the 5-s period around this transition in Fig. 27. A further graph of the vertical pitch and yaw angles for this period is provided in Fig. 28. Figure 27 highlights the very abrupt nature of this particular transition. The predominant pitch change occurs between $t = 415.74$ and 416.25 s, when the pitch- angle changes from 26.2 to 82.40 deg. During this period, the vertical pitch angle increases from −63.4 to 1.0 deg, after which it reaches a maximum value of 13.3 deg, providing dynamic braking to allow the vehicle to wash off excess translational velocity. At the start of this maneuver, the U, V, and W velocity components are 110.3, −13.3, and 26.2 ft/s; at the end of the sharp pitch change, they are 31.78, −17.85, and 82.37. Ignoring wind,[***] this final value corresponds to an angle of attack of 68.7 deg. Over the abrupt pitch change part of the maneuver, the total altitude gain is 17.0 ft. The reason for the extreme abruptness of the pitch-up is believed to be associated with a dynamic stall of the rear (high aspect ratio) main wing under low-throttle conditions, which then conveniently allows the back of the vehicle to "fall under" the nose, leaving the vehicle in a vertical attitude. The abrupt pitch change and dynamic braking parts of the maneuver are clear in the reconstructed vehicle plots provided in Fig. 29, which shows the vehicle attitude and velocity vector at 0.5-s time increments between

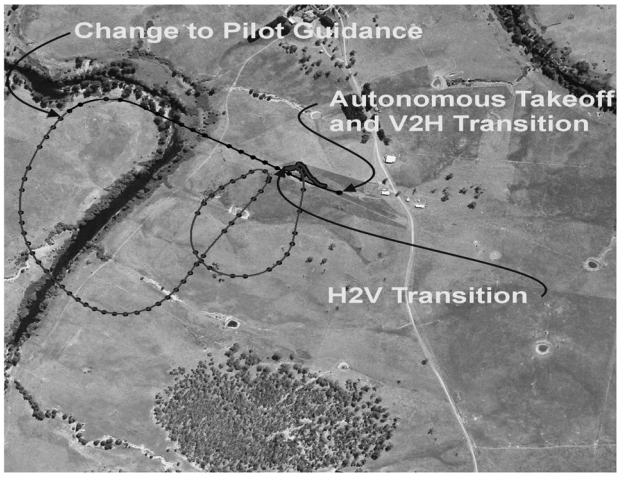

Fig. 25 Flight path on 30 August 2006 in Marulan, New South Wales, Australia (circles represent GPS readings).

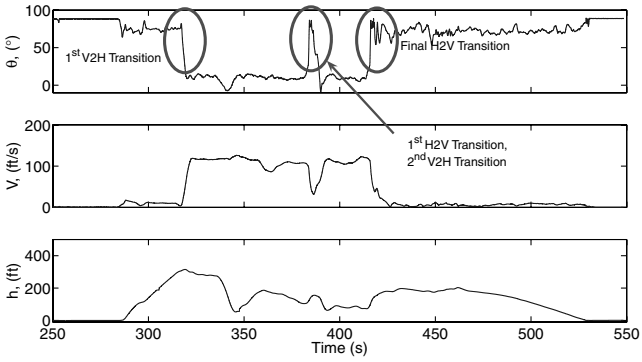

Fig. 26 Pitch angle, velocity, and altitude for flight on 30 August 2006.

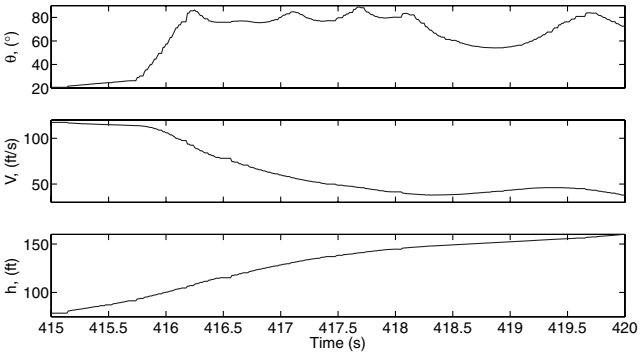

Fig. 27 Details of pitch angle, velocity, and altitude for flight on 30 August 2006 at the point of the second H2V transition.

[§§]Videos of this and other T-wing flights can be found at http://www.aeromech.usyd.edu.au/uav/twing [retrieved 24 Sept. 2007].

[¶¶]The dwell time at vertical waypoints was reduced for this flight from the 6 s used previously.

[***]The vehicle was not equipped with an air data probe.

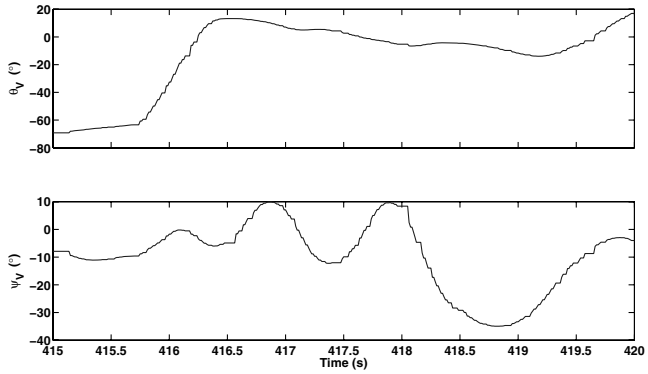

Fig. 28 Vertical Euler tilt angles during transition; lateral oscillations are clear (flat spots in the graphs indicate missed data points.)

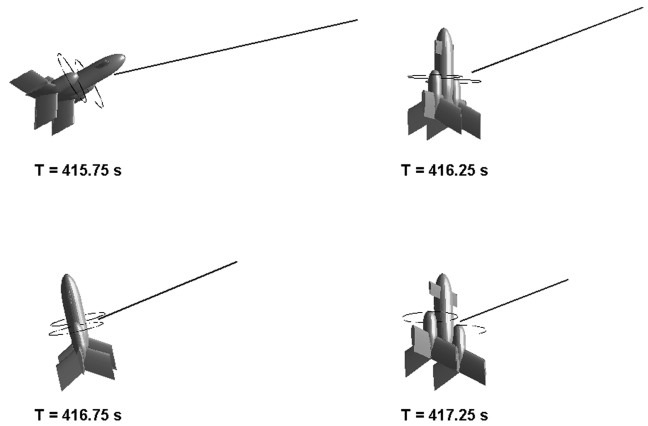

Fig. 29 Transition attitude and velocity vector at 0.5-s intervals (reconstructed from flight test data); the length of the velocity vector is scaled with respect to the vehicle size to represent the distance traveled in 1/10 of a second.

$t = 416.75$ and 418.25 s. Note that the dynamic braking is an intentional part of the maneuver. The last frame in this sequence also shows the yaw instability at the top of the transition (discussed later).

In comparison with the simulation results (Fig. 15), the pitch change is more rapid and the altitude gain is significantly less. Although the results are not directly comparable,[†††] the differences suggest that there may be some important discrepancies in the simulation database that affect this transition. For instance, the simulation shows a small pitch oscillation as the vehicle passes through 70 deg during the transition, which is not seen in the test. Such discrepancies are not altogether unexpected, because it was always known that the database would have problems at high-speed poststall angles (approximately the shaded region in the trim graph in Fig. 4).

C. Oscillations at the End of the H2V Transition

In the graphs of pitch angle, some oscillations are observed after the completion of the H2V maneuver. These are, in fact, oscillations in the vertical yaw direction, rather than vertical pitch direction, as confirmed by Fig. 28. They are associated with incorrect rudder gain scheduling, which caused the rudder to saturate in both directions at the top of the maneuver. This is because the vehicle was originally equipped with much-lower-quality inertial sensors, for which the velocity estimates would diverge rapidly in the event of a short GPS outage. For this reason and the lack of an air data probe, the original gain scheduling of controllers was based on pitch angles and throttle settings (and the predicted correlation of these back to trim-velocity conditions). This is clearly inappropriate for such a dynamic maneuver as seen here; in this case, the vehicle was using scheduling for standard vertical hover flight, because the pitch angle was approximately vertical, even though it had a translational velocity of 90.1 ft/s. Even though the rudder aerodynamic contributions may be unpredictable under such conditions, the engine throttle-balancing mechanism tied to the rudder deflection is still very effective at these angles of attack and severely underpredicted using its hover values. No oscillations are seen in the slower simulated transition. The fact that no pitch transients are observed at the top of the transition when the low-level translational velocity controllers are engaged suggests that the mechanism outlined in Eq. (8) to perform this mode transition is effective.

[†††]The simulation was done fully autonomously, whereas the flight test was performed with pilot guidance-level input up to the entry point of the maneuver.

VIII. Conclusions

The primary result from flight tests over the last two years is the affirmation of the feasibility of the T-wing tail-sitter concept. The vehicle was flown autonomously from takeoff to landing in vertical flight in the presence of considerable winds with success. It has also completed all portions of the complete flight envelope, including transition maneuvers, though with the necessity of pilot guidance-level input during the H2V transition and landing phases. The current control structure, which uses an amalgam of simple controllers for the different primary flight phases, has proved adequate to tackle the control problem. In addition to some specific fixes for known control issues, the main problem observed with this particular structure is that it requires the presence of significant mode-control logic and special consideration to be given to controller switching. The flight tests also demonstrate that the aerodynamic modeling used to build the simulation is at least accurate enough for control design purposes, though certain particular discrepancies were observed between test and simulation results.

Future work will concentrate on achieving autonomous flight through the complete flight envelope when time and funding permit. The most obvious area requiring improvement is the yaw oscillation at the top of the H2V transition. This will be done by improving the gain scheduling of rudder controllers to account for the effect that significant W velocities have on rudder effectiveness, due to the presence of the rudder-to-differential throttle interconnect. Because the current higher-quality inertial system is able to withstand much longer GPS outages, the full velocity-state information can be used. The addition of a dedicated air data system will also facilitate the prediction of velocity-state information, though it is unlikely that a low-cost sensor would handle the extreme angles of attack observed during the H2V transition reliably. The maneuver itself may be refined to limit the angles of attack reached, though with the penalty of greater height gained. This would be done by increasing entry speed and throttle profile during the maneuver. With a demonstrated steady-state descent velocity of 4 ft/s, an extra 300 ft of altitude gain comes at the cost of an extra 75 s of descending flight.

For hover-mode flight, improvements to the guidance and control strategies through the use of a quaternion formulation of attitude will be considered, as is done in the transition mode. The use of a model-predictive control strategy will also be assessed in an effort to eliminate the multiplicity of different controllers in use. (Initial vertical mode flights have been conducted.) Finally, parameter identification work, particularly in hover flight in strong-winds, is needed to establish the quality of the aerodynamic modeling. This would allow deficiencies to be identified and controllers to be improved.

Acknowledgments

This work would not have been possible without a grant from the U.S. Air Force Office of Scientific Research (AFOSR), contract number FA5209-04-P-0563, which was instrumental in purchasing the much-higher-precision real-time kinematic global positioning system sensor with inertial measurement unit interface that has enabled fully autonomous flights on the tether test rig. The

continued support of Sonacom Pty, Ltd., in this project is also acknowledged.

References

[1] Stone, R. H., "Configuration Design of a Canard Configured Tail-Sitter Unmanned Air Vehicle Using Multidisciplinary Optimisation," Ph.D. Dissertation, Dept. of Aeronautical Engineering, Univ. of Sydney, Sydney, Australia, 1999.

[2] Stone, R. H., "The T-Wing Tail-Sitter Research UAV," 2002 Biennial International Powered Lift Conference and Exhibit, AIAA Paper 2002-5970, 2002.

[3] Stone, R. H., and Wong, K. C., "Preliminary Design of a Tandem-Wing Tail-Sitter UAV Using Multi-Disciplinary Optimisation," *AUVSI '96 Proceedings*, Vol. 1, Association of Unmanned Vehicle Systems International, Arlington, VA, 1996, pp. 163–178.

[4] Albion, N., "Vertically Launchable and Recoverable Winged Aircraft," The Boeing Company, Chicago, IL, U.S. Patent No. 5765783, 1998.

[5] Munson, K., *Jane's Unmanned Aerial Vehicles and Targets*, Jane's Information Group, Surrey, England, U.K., 1998.

[6] Bridgman, L., *Jane's All The World's Aircraft 1954–55*, Jane's All The World's Aircraft Publishing, London, 1955, p. 227.

[7] Bridgman, L., *Jane's All The World's Aircraft 1955–56*, Jane's All The World's Aircraft Publishing, London, 1956.

[8] McCormick, B. W., *Aerodynamics of V/STOL Flight*, Dover, Mineola, NY, 1999.

[9] Cycon, J. P., Rosen, K. M., and Whyte, A. C., "Unmanned Flight Vehicle Including Counter Rotating Rotors Positioned Within a Toroidal Shroud and Operable to Provide all Required Vehicle Flight Controls," United Technologies Corp., Hartford, CT, U.S. Patent No. 5152478, 1992.

[10] Avanzini, G., Ciniglio, U., and de Matteis, G., "Full-Envelope Robust Control of a Shrouded-Fan Unmanned Vehicle," *Journal of Guidance, Control, and Dynamics*, Vol. 29, No. 2, 2006, pp. 435–443.

[11] Johnson, E. N., and Turbe, M. A., "Modeling, Control, and Flight Testing of a Small Ducted-Fan Aircraft," *Journal of Guidance, Control, and Dynamics*, Vol. 29, No. 4, 2006, pp. 769–779.

[12] Knoebel, N. B., Osborne, S. R., Snyder, D. O., McLain, T. W., Beard, R. W., and Eldredge, A. M., "Preliminary Modeling, Control, and Trajectory Design for Miniature Autonomous Tailsitters," AIAA Guidance, Navigation, and Control Conference, Keystone, CO, AIAA Paper 2006-6713, 2006.

[13] Johnson, E. N., and Kannan, S. K., "Adaptive Trajectory Control for Autonomous Helicopters," *Journal of Guidance, Control, and Dynamics*, Vol. 28, No. 3, 2005, pp. 524–538.

[14] Carrington, C. K., and Junkins, J. L., "Optimal Nonlinear Feedback Control for Spacecraft Attitude Maneuvers," *Journal of Guidance, Control, and Dynamics*, Vol. 9, No. 1, 1986, pp. 99–107.

[15] Junkins, J. L., Akella, M. R., and Robinett, R. D., "Nonlinear Adaptive Control of Spacecraft Maneuvers," *Journal of Guidance, Control, and Dynamics*, Vol. 20, No. 6, 1997, pp. 1104–1110.

[16] Vidali, S. R., Kraige, L. G., and Junkins, J. L., "New Results on the Optimal Spacecraft Attitude Maneuver Problem," *Journal of Guidance, Control, and Dynamics*, Vol. 7, No. 3, 1984, pp. 378–380.

[17] Klumpp, A. R., "Singularity-Free Extraction of a Quaternion from a Direction-Cosine Matrix," *Journal of Spacecraft and Rockets*, Vol. 13, No. 12, 1976, pp. 754–755.

[18] Kubo, D., and Suzuki, S., "Transitional Flight Control of Tail-Sitter Vertical Takeoff and Landing Mini Unmanned Aerial Vehicle," AIAA Infotech@Aerospace 2007 Conference and Exhibit, Rhnert Park, CA, AIAA Paper 2007-2752, 2007.

[19] Stevens, B. L., and Lewis, F. L., *Aircraft Control and Simulation*, 1st ed., Wiley, New York, 1992.

[20] Stone, R. H., "Aerodynamic Modelling of a Wing-in-Slipstream Tail-Sitter UAV, 2002 Biennial International Powered Lift Conference and Exhibit, AIAA Paper 2002-5951, 2002.

[21] Stone, R. H., "Aerodynamic Modelling of the Wing-Propeller Interaction for a Tail-Sitter UAV," *Journal of Aircraft* (to be published).

[22] Shuster, M. D., "A Survey of Attitude Representations," *Journal of the Astronautical Sciences*, Vol. 41, No. 4, 1993, pp. 439–517.

[23] Phillips, W. F., Hailey, C. E., and Gebert, G. A., "Review of Attitude Representations Used for Aircraft Kinematics," *Journal of Aircraft*, Vol. 38, No. 4, 2001, pp. 718–737.

[24] Hale, F. J., *Introduction to Aircraft Performance, Selection and Design*, 1st ed., Wiley, New York, 1984.

[25] Blakelock, J. H., *Automatic Control of Aircraft and Missiles*, 2nd ed., Wiley, New York, 1991.

[26] Etkin, B., *Dynamics of Atmospheric Flight*, 1st ed., Wiley, New York, 1972.

[27] Stone, R. H., "Control Architecture for a Tail-Sitter Unmanned Air Vehicle," *5th Asian Control Conference*, Vol. 2, Inst. of Electrical and Electronics Engineers, Piscataway, NJ, 2004, pp. 736–744.

[28] Stone, R. H., "Design Considerations for a Wing-in-Slipstream Tail-Sitter Unmanned Air Vehicle (UAV)," *10th Australian International Aerospace Congress*, Royal Aeronautical Society, Australian Div., 2003, Paper aiac2003-068.

[29] Gavrilets, V., Mettler, B., and Feron, E., "Human-Inspired Control Logic for Automated Maneuvering of Miniature Helicopter," *Journal of Guidance, Control, and Dynamics*, Vol. 27, No. 5, 2004, pp. 752–759.

[30] Stone, R. H., "Transition Maneuver Optimization for the T-Wing Tail-Sitter UAV," *10th Australian International Aerospace Congress*, Royal Aeronautical Society, Australian Div., 2003, Paper aiac2003-069.